Water Science & Technology

IWA PUBLISHING

Water Science & Technology Vol 90 No 3, 935 doi: 10.2166/wst.2024.250

Urban flood-bearing vulnerability evaluation based on the moment estimate weighting and improved gray target model

Dengming Yan[a,b], Liu Su[a], Simin Liu[c,*], Hong Lv[a,b], Jin Lin[c], Zhilei Yu[d] and Lucong Cao[c]

[a] Yellow River Engineering Consulting Co., Ltd, Zhengzhou 450003, China
[b] Key Laboratory of Water Management and Water Security for Yellow River Basin, Ministry of Water Resources (Under Construction), Zhengzhou 450003, China
[c] Development Research Center, National Forestry and Grassland Administration, Beijing 100714, China
[d] School of Water Conservancy and Transportation, Zhengzhou University, Zhengzhou 450001, China
*Corresponding author. E-mail: 13253610702@163.com

ABSTRACT

Increasingly severe flooding seriously threatens urban safety. A scientific urban flood-bearing vulnerability assessment model is significant to improve urban risk management capacity. The gray target model (GTM) has advantages in urban flood-bearing vulnerability assessment. However, indicator correlation and single bull's-eye are commonly neglected, leading to defective evaluation results. By integrating the four base weights, an improved weighting method based on the moment estimate was proposed. Then, the marginal distance was used to quantify the indicator correlation, and the TOPSIS model was introduced to define the relative bull's-eye distance. Thus, an improved gray target evaluation method was established. Finally, an urban flood-bearing vulnerability evaluation model was presented based on the moment estimate weighting-improved GTM. In this study, Zhengzhou City, China, was taken as an example. The spatial and temporal changing characteristics of the flood-bearing vulnerability of Zhengzhou from 2006 to 2020 were investigated. The results show that: (1) On the temporal scale, the disaster-bearing vulnerability of Zhengzhou City showed an upward trend during the 15 years; (2) On the spatial scale, Guancheng District of Zhengzhou City had the relatively highest vulnerability to urban flooding. This study is expected to provide a scientific reference for urban flood risk management.

Key words: disaster prevention and mitigation, flood-bearing vulnerability, gray target model, moment estimate empowerment, urban flood

HIGHLIGHTS

- Rising vulnerability to urban flooding due to climate extremes and urbanization.
- Comprehensive urban flood-bearing vulnerability assessment.
- An improved gray target evaluation model.
- The optimal weights based on the idea of moment estimation.
- An upward trend of the vulnerability to disasters in Zhengzhou City.

1. INTRODUCTION

Floods are one of the most widespread and costly natural disasters worldwide (Gu *et al.* 2020; Liu *et al.* 2022; Rentschler *et al.* 2022). According to the 2021 Global Natural Disaster Assessment Report, flood events had the highest frequency during 2000–2021, accounting for 51% of extreme weather events and 62.7% of the number of people affected. The impacts of rapid urbanization on urban hydrology are becoming more pronounced, increasing urban drainage vulnerability (Zhang *et al.* 2018; Shukla & Gedam 2019; Pang *et al.* 2022). Urbanization also leads to highly concentrated social assets and significantly increases flood vulnerability (Wing *et al.* 2020; Chen *et al.* 2021; Wang *et al.* 2023; Yang *et al.* 2023). Urban management is challenged with increasing urban flooding risks in flood prevention, hindering sustainable urban development (Kang *et al.* 2023; Li *et al.* 2023a; Zia *et al.* 2023). As an important tool for flood disaster prevention, urban flood vulnerability assessment has significant practical value in flood risk management to reduce urban flood damage.

On 20 July 2021, a world-shattering flooding event occurred in Zhengzhou City, China. This extreme flooding event resulted in severe inundation, greatly impacting the city (Zheng *et al.* 2022). The flood caused 380 deaths, affected 1.9 million people and induced direct economic losses of 40.6 billion yuan (MEMPRC 2022). The rainfall on the day (552.5 mm)

accounted for 86.2% of the annual average rainfall (640.8 mm) in Zhengzhou City. The maximum hourly rainfall (201.9 mm) broke the historical record since the establishment of Zhengzhou Railway Station in 1951 and also set a new record for meteorological observations in mainland China (Zheng *et al.* 2022). This rainfall event triggered many types of flooding disasters, such as urban flooding, river overflow and dike breach, and emergency discharge from reservoirs, and exposed the inefficiency of urban flood risk management (Dong *et al.* 2022a; Tu *et al.* 2023; Yang *et al.* 2023). Therefore, it is important to construct an efficient and accurate flooding vulnerability assessment method in order to improve the disaster emergency response capacity of Zhengzhou City.

Urban flooding disaster is characterized by the extent of damage caused by heavy rainfall disaster-causing factors on the urban disaster-bearing body after urban flooding vulnerability exceeds a certain threshold. The disaster-bearing body shows a certain degree of resilience in response to flooding. Thus, flood-bearing vulnerability is a collection of urban socio-economic factors and disaster prevention facilities. Currently, there are various forms of vulnerability assessment methods. For example, Darlington *et al*. (2022) used historical flood data for the past 25 years in Calgary, Canada, combined with vulnerability indicators (flood loss, postsecondary education level, recent movers, etc.), methodology to predict future social vulnerability trends, and found that residential values in high flood hazard areas increase residential values faster than low flood hazard areas; Xing *et al.* (2023) used streetscape and remote sensing imagery to estimate urban building flood vulnerability in Hefei City, China, and found that multi-source datasets are fused to improve building vulnerability assessment; Zhang *et al.* (2022) used the coupled one- and two-dimensional hydrodynamic model MIKE FLOOD to simulate flood vulnerability of the city of Zhengzhou, China to simulate flood vulnerability of the city of Zhengzhou, China. The results showed that the scenarios with higher vulnerability were mostly short-term rainstorms with significant spatial and temporal distribution. In conclusion, the trend analysis method is not suitable for areas where effective historical data is lacking. Remote sensing image data are often limited by spatial and temporal accuracy. Storm water flood simulation models are complicated to construct and are mostly applicable to small spatial scales.

The indicator system method is widely used in flood vulnerability assessment because it examines the risk situation of heavy rainfall and flooding from multiple aspects, with easy access to data and strong operability. For example, Bucherie *et al.* (2022) developed a social vulnerability index assessment methodology for flooding in Ecuador using indicators for vulnerable groups, socioeconomics, health, and education, combined with principal component analysis and expert knowledge. The index driven by principal component analysis was found to indicate a higher level of relative vulnerability than the expert results. Langlois *et al.* (2023) constructed a flood vulnerability assessment framework incorporating indicators of current, internal, and biophysical vulnerability of cities, and its application in Indonesia showed that Banten, Jakarta, West Java, and Central Java are susceptible to flood-related damages. Yang *et al.* (2023) used population and GDP indicators to predict flood exposure risk in Chaohu City, China, under future scenarios, and found that population-intensive and GDP-intensive areas are more vulnerable to flood exposure than other areas.

The indicator system method utilizes hazard elements as evaluation factors, combines mathematical methods to determine weights, and finally, assigns a comprehensive evaluation value (Jibhakate *et al.* 2023). Indicator weight is one of the most important factors affecting vulnerability evaluation. Three methods are commonly used to determine weights. The subjective assignment method (Lyu *et al.* 2020; Ramkar & Yadav 2021; Ye *et al.* 2023) includes the analytical hierarchy process (AHP) and the order relationship analysis (G1) method. They have the advantage of expert experience but are greatly influenced by human factors. The objective assignment method (Xu *et al.* 2018; Ziarh *et al.* 2021; Ye *et al.* 2023) includes the entropy weight (EW) and the inter-criteria correlation (CRITIC) methods. They can avoid subjective arbitrariness, excluding subjective advantages. The comprehensive assignment method (Lai *et al.* 2015; Wang *et al.* 2018; Peng & Zhang 2022; Ye *et al.* 2023) includes the multiplier synthesis method and the empirical coefficient method. These assignment methods use the weighting method to integrate subjective and objective weights. It has been found that the multiplier effect of the multiplier synthesis method was larger with smaller indicator weights. The empirical coefficient method is subjective and can overcome this effect. Therefore, determining indicator weights is one of the problems to be solved in vulnerability assessment models.

The core idea of the gray target model (GTM) is to set an optimal goal under the condition that there is no standard model and to take the distance from each scheme to the bull's-eye as the evaluation value of the scheme (Jin *et al.* 2020; Qin *et al.* 2022; Zhu & Wen 2023). With its simple principle and clear evaluation process, the GTM has been widely used in disaster risk assessment, environmental evaluation, and multi-objective decision-making (Li *et al.* 2018; Jin *et al.* 2020; Tansar *et al.* 2023; van Schaik *et al.* 2023), with reasonable and accurate evaluation results and significant development prospects. Scale correlation inevitably exists between multiple indicators in the indicator system method (Jiang *et al.* 2019; Sun *et al.* 2022; Ji

et al. 2023). Existing gray target models often adopt Euclidean distance to solve the bull's-eye distance and ignore this feature. Traditional models only use the optimal value as a single bull's-eye, leading to an insignificant order of the scheme advantages and disadvantages when the bull's-eye distance of multiple schemes is the same or similar. In actual evaluation, due to the complex relationship between the indicators, the single bull's-eye is insignificant in explaining the evaluation results.

In order to scientifically diagnose urban flood-bearing vulnerability and improve the defects of multi-indicator assessment methods, the urban flood-bearing vulnerability assessment system was proposed in this article consists of three parts: Based on the socio-economic factor of the city, a new urban flood-bearing vulnerability indicator system was constructed (Section 3.2); Based on the correlation coefficient matrix of the Mahalanobis distance (Du *et al.* 2017; Chen *et al.* 2023; Ji *et al.* 2023) and the relative bull's-eye distance, an improved gray target evaluation model was proposed for evaluating the vulnerability of different scenarios, which improved the insignificant order of advantages and disadvantages in the traditional method (Section 3.3); Using the idea of distance estimation, a distance estimation empowerment method integrating multiple weights was put forward, which overcomes the contingency and inexperience of the single weights (Section 3.4).

2. STUDY AREA AND DATA SOURCES

2.1. Study area

Zhengzhou is a representative city in the North China Plain, and its main urban area includes Huiji, Zhongyuan, Erqi, Jingshui, and Guancheng Districts (Figure 1). The resident population exceeds 10 million, the total GDP exceeds one trillion Chinese yuan (more than $137.6 billion), and the urban area is 1,010 km^2. During the rapid urbanization stage at the beginning of the 21st century, the built-up area expanded rapidly from 137.5 to 549.3 km^2, with an urbanization rate of over 70%. The annual average rainfall is 542.15 mm, with 65% concentrated in summer due to the temperate monsoon climate. The center of heavy rainfall is mostly located in the central urban area. Consequently, this area is extremely vulnerable to urban flooding every summer (Li *et al.* 2023b). Therefore, it is necessary to analyze the spatial and temporal characteristics of urban flood-bearing vulnerability in order to support the early warning of urban flooding risk.

2.2. Data sources

The city socio-economic data in this article was obtained from the Zhengzhou Municipal Bureau of Statistics (https://tjj.zhengzhou.gov.cn/). The road network data was obtained from the official website of OpenStreetMap (https://www.

Figure 1 | Location distribution of the study area (Zhengzhou City).

openstreetmap.org). The river network data was from the National Center for Basic Geographic Information (http://www.ngcc.cn/ngcc/).

3. METHODS

3.1. Research framework

In order to accurately determine the urban flooding vulnerability, this article attempted to construct an urban flood-bearing vulnerability evaluation model based on the moment estimate weighting and improved gray target (Figure 2). First, the urban flood-bearing indicator system was constructed (Section 3.2). Second, an improved GTM based on the Mahalanobis distance and double bull's-eye was proposed (Section 3.3). In addition, the moment estimation method was used to determine more balanced integration weights (Section 3.4).

3.2. Urban flood-bearing vulnerability indicator and standardization

3.2.1. Urban flood-bearing vulnerability indicator system

As the urban economy develops, urban flooding vulnerability increases. Urban investment in disaster prevention and relief also increases. Thus, urban flood-bearing capacity is strengthened. Urban flood-bearing vulnerability is expressed as the resilience of the disaster-bearing body to reduce the impact of flooding (Zhang *et al.* 2018; Rentschler *et al.* 2022; Wang *et al.* 2023; Yang *et al.* 2023). At a higher urban economic level, urban flooding vulnerability is larger. At a stronger disaster prevention and relief capacity, urban flood-bearing vulnerability is lower. Therefore, these two elements interact and provide feedback, both characterized by the flood-bearing vulnerability. The urban flood-bearing vulnerability indicators (Table 1) were constructed by considering urban socio-economic development factors, such as urban socio-economics, population size, degree of development (Li *et al.* 2023a, 2023b; Yang *et al.* 2023), urban disaster prevention, and mitigation implementation level and subsurface (Wahalathantri Buddhi *et al.* 2016; Kim *et al.* 2021).

3.2.2. Standardization of indicators

Due to the unit differences in different indicators, it is necessary to standardize each index into the same dimensional value on $0 \sim 1$, as shown in Equation (1). The normalized v_{ij}^{+} and v_{ij}^{-} of the positive and negative indicators form the evaluation matrix R. R $(m \times n)$ contains m evaluation schemes and n evaluation indicators. As the input of the evaluation model and the weighting method, R directly participates in the calculation of flood-bearing vulnerability assessment, and finally obtains

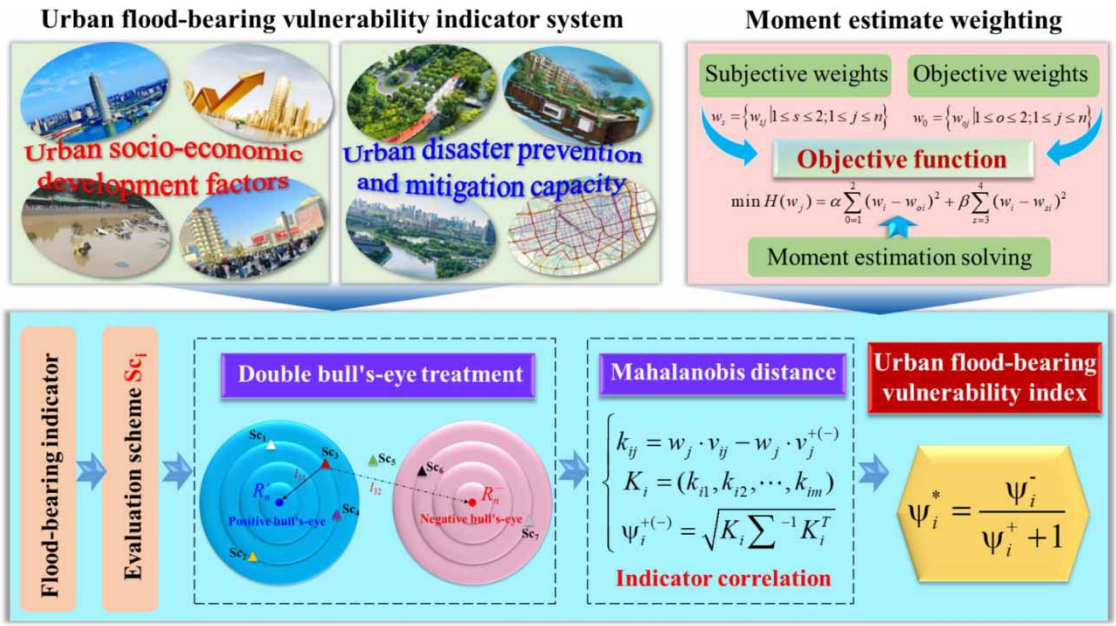

Figure 2 | Research framework diagram.

Table 1 | Urban flood-bearing vulnerability indicator system

Category	Indicator	Connotation
Urban socio-economic development factors	GDP per land (A1)	Key elements of disaster impacts and urban functioning
	Population density (A2)	Highest priority for disaster relief
	Fixed asset investment (A3)	Urban economic structure and productivity distribution
	Construction land area ratio (A4)	Characterizing the spatial condition of urban imperviousness
	Financial revenue and expenditure ratio (A5)	Government capacity for disaster relief and assistance
Urban flood prevention and mitigation capacity	Greening rate (B1)	Indicating urban infiltration and flood mitigation capacity
	Drainage pipe network density (B2)	Most important flood control measures
	Road network density (B3)	Reflecting disaster response capacity
	River network density (B4)	Secondary urban flood drainage system
	Number of medical staff (B5)	Reflecting the capacity of urban healthcare

the vulnerability value of each evaluation scheme m. Taking Zhengzhou as the study area, one-year flood-bearing vulnerability dataset is an evaluation scheme, and each evaluation scheme contains 10 indicators shown in Table 1. Finally, the urban flood-bearing vulnerability for each year is obtained.

$$\begin{cases} v_{ij}^{+} = (x_{ij}^{+} - x_{\min})/(x_{\max} - x_{\min}) \\ v_{ij}^{-} = (x_{\max} - x_{ij}^{-})/(x_{\max} - x_{\min}) \end{cases} \tag{1}$$

where i is the evaluation scheme, $i = 1 \sim m$; j is the evaluation indicator, $j = 1 \sim n$; x_{ij}^{+} and x_{ij}^{-} are the positive and negative driving indicators, respectively. v_{ij}^{+} and v_{ij}^{-} are normalized values for x_{ij}^{+} and x_{ij}^{-}, respectively.

3.3. Improved GTM

3.3.1. GTMs and disadvantages

The GTM is a traditional multi-attribute evaluation method (Fu *et al.* 2021; Ding & Liu 2023; van Schaik *et al.* 2023), which sets the optimal value target center with no standard pattern and uses the distance from each scheme to the target center as the evaluation index. The target distance of different schemes is used to achieve the ranking of superiority or inferiority:

$$\psi_i^{*} = \sqrt{\frac{1}{n}\sum_{i=1}^{n}(v_{ij} - v'_j)^2} \tag{2}$$

where ψ_i^{*} represents the target distance of scheme v_{ij}; n is the number of schemes; and v'_{ij} is the target scheme (generally a set of optimal values for each indicator).

Traditional GTM have the following problems:

Traditional GTM use only the optimal value as a single target center. When target distances of multiple schemes are the same or close, the interpretation of evaluation results is insignificant. When the target distances from the optimal value are the same or close, the distances from the worst target center often differ significantly, resulting in significant differences in evaluating the superiority or inferiority of the schemes.

Indicator correlations inevitably exist in an evaluation system. Traditional GTM use the Euclidean distance to calculate target distances, ignoring indicator correlations. In contrast, the Mahalanobis distance considers the covariance between indicators, reflecting the deviation of two indicators from their respective means. The Mahalanobis distance also uses correlation coefficients to fully describe the degree of correlation between indicators.

If $1/n$ is considered as the weight of the indicators, the target distance is the square root of the sum of the weighted target center coefficients for each indicator. This assumes that the indicators are of equal importance, which may not accurately reflect the actual situation.

3.3.2. Creating a positive and negative double bull's-eye based on TOPSIS

GTM only take the optimal value as the bull's-eye. There are insignificant differences in the evaluation values when multiple schemes are at similar distances from the bull's-eye (Ji *et al.* 2023). Typically, when different schemes are close to the optimal center, the distance to the worst scheme varies greatly. Similar evaluation values cannot reflect this situation. Figure 3 shows that when Schemes Sc_2 and Sc_3 have the same positive bull's-eye distances l_{21} and l_{31}, their negative bull's-eye distances l_{22} and l_{32} differ dramatically, i.e., $l_{21} = l_{31}$, $l_{22} > l_{32}$. Therefore, the defects of different schemes corresponding to a single target center are significant.

TOPSIS is to rank the evaluation programs by comparing their proximity to the 'positive ideal solution' and the 'negative ideal solution', and the positive ideal solution in the TOPSIS method is the collection of the optimal values of all evaluation indexes, and all its attributes are optimal; the positive ideal solution is the collection of the worst values, and all its attributes are the worst. Hence, the positive ideal solution introduced into the TOPSIS model is defined as the positive bull's-eye R_n^+ (Equation (3)), and the negative ideal solution is defined as the negative bull's-eye R_n^- (Equation (4)):

$$R_n^+ = (v_1^+, \ldots, v_j^+, \ldots, v_n^+) \tag{3}$$

$$R_n^- = (v_1^-, \ldots, v_j^-, \ldots, v_n^-) \tag{4}$$

where v_j^+ and v_j^- are the maximum and minimum values of the jth evaluation indicator in the m schemes, respectively.

3.3.3. Improvement of indicator correlation based on the Mahalanobis distance

In the comprehensive evaluation system, correlations between indicators are inevitable, such as the urban economy and the level of integrated facility construction (Jiang *et al.* 2019; Sun *et al.* 2022; Ji *et al.* 2023). Traditional gray target models use Euclidean distance to solve the bull's-eye distance, ignoring the correlation between indicators. The Mahalanobis distance considers the covariance between indicators, characterizing the degree of deviation of two indicators from their respective means. The correlation coefficient is utilized to fully describe the degree of correlation between the indicators (Ji *et al.* 2023). Therefore, based on the correlation coefficient matrix, the bull's-eye distances from the program Sc_i to the positive and negative bull's-eyes were established, respectively.

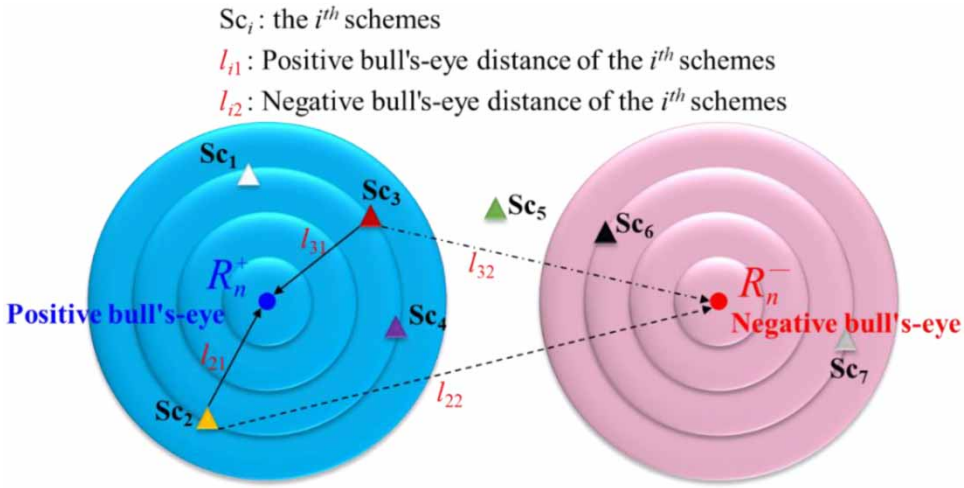

Figure 3 | Schematic of positive and negative bull's-eye distance.

Positive bull's-eye distance ψ_i^+ is expressed as

$$\begin{cases} k_{ij} = w_j \cdot v_{ij} - w_j \cdot v_j^+ \\ K_i = (k_{i1}, k_{i2}, \ldots, k_{im}) \\ \psi_i^+ = \sqrt{K_i \sum^{-1} K_i^T} \end{cases} \tag{5}$$

where k_{ij} is the positive bull's-eye distance of Sc_i; w_j is the weight of the jth evaluation indicator, determined using moment estimate weighting in Section 3.4; K_i is the weighted difference matrix from Sc_i to the positive bull's-eye; and Σ is the matrix of correlation coefficients for K.

Negative bull's-eye distance ψ_i^+ is expressed as

$$\begin{cases} h_{ij} = w_j \cdot v_{ij} - w_j \cdot v_j^- \\ H = (h_{i1}, h_{i2}, \ldots, h_{im}) \\ \psi_i^- = \sqrt{H_i \sum^{-1} H_i^T} \end{cases} \tag{6}$$

where h_{ij} is the negative bull's-eye distance of Sc_i; and H_i is the weighted difference matrix from Sc_i to the negative bull's-eye.

3.3.4. Urban flood-bearing vulnerability index based on the relative bull's-eye distance

To address the inconsistencies in evaluating the single positive and negative bull's-eye distances, the relative bull's-eye distance was used to establish an urban flood-bearing vulnerability index (Equation 7). A larger s means that Sc_i is closer to the positive bull's-eye and farther away from the negative bull's-eye, i.e., the flood-bearing vulnerability index of Sc_i is lower; otherwise, the flood-bearing vulnerability is higher.

$$\psi_i^* = \frac{\psi_i^-}{(\psi_i^+ + 1)} \tag{7}$$

It is necessary to add 1 to the denominator in Equation (7) to avoid a positive bull's-eye distance of 0.

3.4. Moment estimate weighting

Indicator weights are commonly the key to the vulnerability evaluation system (Bucherie *et al.* 2022). Existing comprehensive assignment methods are equalization methods combining the advantages of subjective or objective assignment and have the advantage of being widely applied (Jiang *et al.* 2019; Wen *et al.* 2021; Ye *et al.* 2023). However, they have the disadvantages of multiplier effect or subjectivity.

3.4.1. Moment estimation

Moment estimation theory is a statistical method that uses sample moments to estimate overall moments (Adekunle *et al.* 2020; Dong *et al.* 2022b; He & Peng 2022). Moment estimation is not only applicable to scenarios with fewer samples, but is also not affected by large inter-sample deviations. Multiple weights make up a statistical sample, and the idea of moment estimation can be used to determine an overall mean as an integrated optimization weight. It reflects the relative importance in the indicator system and also integrates subjective experience and objective statistical advantages.

3.4.2. Base weight set

The subjective weight determination methods involved are AHP and G1. AHP is a multi-objective decision-making method that calculates the ranking of indicators through the fuzzy quantization method of qualitative indicators, and its determined weight is w_{s1}. The G1 method is a rational assignment of the degree of importance of indicators through the experts' evaluation of the ordinal relationship of each indicator at the same level, and its determined weight is w_{s2}.

The objective weight determination methods involved are EW and CRITIC methods. The EW method is a system analysis method that takes the entropy value as the weight by measuring the degree of disorder of the complex multi-indicator system, and its determined weight is w_{o1}. CRITIC is a weight-solving method that comparing the degree of variability and conflict of the multi-indicator system, and its determined weight is w_{o2}. They need to satisfy non-negativity and are normalized to form

the base weight set w_{so}:

$$w_{so} = \{w_s, w_o \mid 1 \le s \le 4; 1 \le j \le n\} \tag{8}$$

where so is the number of the weight set; $0 \le w_{so} \le 1$.

3.4.3. Solving the objective function for the optimal weights

Smaller deviations between the four weight vectors and the combination weight were better in order to obtain the optimal weight vector $w' = \{w_1, \ldots w_j, \ldots w_n\}$. For different evaluation objectives, the proportion of subjective and objective weights is different, which are represented by α and β, respectively. Thus, the objective function to be solved for the optimal weights is

$$\min H(w_j) = \alpha \sum_{o=1}^{2} (w_i - w_{oi})^2 + \beta \sum_{s=3}^{4} (w_i - w_{si})^2 \tag{9}$$

The steps to solve the optimal weights are as follows:

Step 1: According to the basic concept of moment estimation, the expected values of w_{oj} and w_{sj} are

$$\begin{cases} E(w_{oj}) = \dfrac{\sum_{o=1}^{2} w_{oj}}{2} \\ E(w_{sj}) = \dfrac{\sum_{s=3}^{4} w_{oj}}{2} \end{cases} \tag{10}$$

Step 2: The importance coefficients for w_{oj} and w_{sj} are obtained using

$$\begin{cases} \alpha_j = \dfrac{E(w_{oj})}{E(w_{oj}) + E(w_{sj})} \\ \beta_j = \dfrac{E(w_{sj})}{E(w_{oj}) + E(w_{sj})} \end{cases} \tag{11}$$

Step 3: For each indicator, it can be regarded as taking n samples in w_{oj} and w_{sj}, respectively. According to the theory of moment estimation, the coefficients α and β of the objective function $H(w_j)$ are expressed as

$$\begin{cases} \alpha = \dfrac{\sum_{j=1}^{n} \alpha_j}{n} \\ \beta = \dfrac{\sum_{j=1}^{n} \beta_j}{n} \end{cases} \tag{12}$$

Step 4: The smaller the objective function $H(w_j)$, the better. Then, $H(w_j)$ is transformed into:

$$\begin{cases} \min H = \{H(w_1), H(w_2), \ldots H(w_n)\} \\ \text{st.} \quad \sum_{j=1}^{n} w_j = 1 \end{cases} \tag{13}$$

where $0 \le w_j \le 1$.

Step 5: The linear weighting of Equation (14) is as follows:

$$\begin{cases} \min H = \sum_{j=1}^{n} \alpha \sum_{o=1}^{2} (w_i - w_{oi})^2 + \sum_{j=1}^{n} \beta \sum_{s=3}^{4} (w_i - w_{si})^2 \\ \text{st.} \quad \sum_{j=1}^{n} w_j = 1 \end{cases} \tag{14}$$

Step 6: By solving the objective function $H(w_j)$ through the Lagrange multiplier method, the optimal weights w_j for each indicator can be obtained:

$$w_j = \frac{\left(\alpha \sum_{o=1}^{2} w_{oj} + \beta \sum_{s=3}^{4} w_{sj}\right)}{4} - \frac{\left(\sum_{j=1}^{n} \left(\alpha \sum_{o=1}^{2} w_{oj} + \beta \sum_{s=3}^{4} w_{sj}\right)\right) - 4}{(n \cdot 4)} \tag{15}$$

4. RESULTS

4.1. Optimal weighting results and comparative analysis

4.1.1. Optimal weighting results

By combining AHP and G1 using expert experience, two subjective weights were calculated. Then, using the data of 10 indicators from 2006 to 2020 in Zhengzhou City, two objective weights were evaluated based on EW and CRITIC. Finally, through moment estimation, the optimal weights were calculated, as shown in Figure 4. Among all indicators, *B*2 had the largest optimal weight (0.135). Drainage pipe network was a direct way to relieve floodwater in the city and thus was empirically judged to be the most important indicator. *A*2 had the second-largest optimal weight. This is because large changes in the population ratio in Zhengzhou City in recent years have induced highly variable population density, leading to large objective weights. Figure 4 shows that the optimal combination weights (OCWs) were basically around the median of the four base weights with a variance of only 0.02, showing good consistency.

4.1.2. Analysis of different integration weights

To demonstrate the OCW performance for moment estimation computation, the weight by the Lagrangian algorithm (WLA) was added to compare their performances, and a comparison of the three errors for all metrics is shown in Figure 5. Overall, the performance of OCW is ahead of WLA across the board because the mean and median values of the three types of errors are smaller. The mean RMSE of OCW is smaller than WLA by 0.016, the mean RMSE is 016% smaller, and the absolute error is less than 0.002. These clearly show that the integrated optimization weights have superior performance, and are the most closely linked and less biased than the individual basis weights.

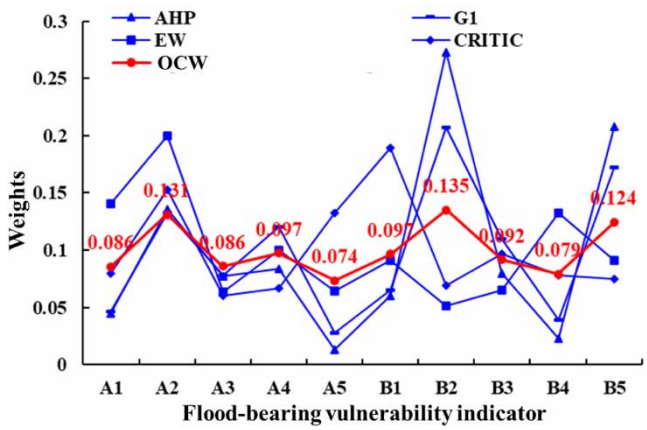

Figure 4 | Weights for flood-bearing vulnerability indicators.

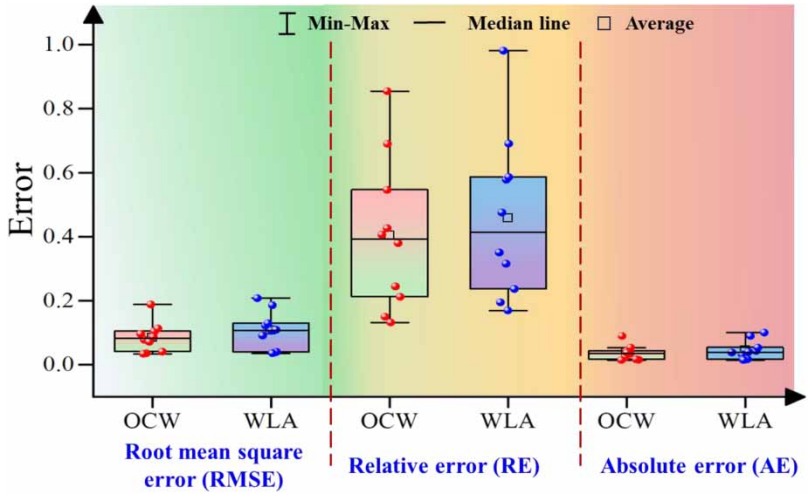

Figure 5 | Comparison of three errors for all indicators for OCW and WLA.

4.2. Temporal changes in flood-bearing vulnerability of Zhengzhou City

In order to visualize the changes in the flood-bearing vulnerability index, the vulnerability index grading criteria based on the natural discontinuity method (Maskrey *et al.* 2019; Feloni *et al.* 2020) is shown in Table 2. Figure 6 shows that over the 11 years, the flood-bearing vulnerability index of Zhengzhou City showed a significant downward trend, i.e., the flood-bearing vulnerability increased. The vulnerability index decreased from 0.62 in 2006 to 0.43 in 2020 (a changing rate of −30.4%), and the vulnerability level rose from medium-hazardous II to second-hazardous III. It can be found that the flooding risk in Zhengzhou City was becoming increasingly severe. There is an urgent need to strengthen disaster prevention and mitigation measures.

Table 2 | Rating criteria for urban flood-bearing vulnerability index

Criteria	Level I (Low)	Level II (Medium)	Level III (Second highest)	Level IV (Highest)
Index range	≧0.80	[0.6, 0.8)	[0.40, 0.60)	<0.40
Color	Blue	Yellow	Orange	Red

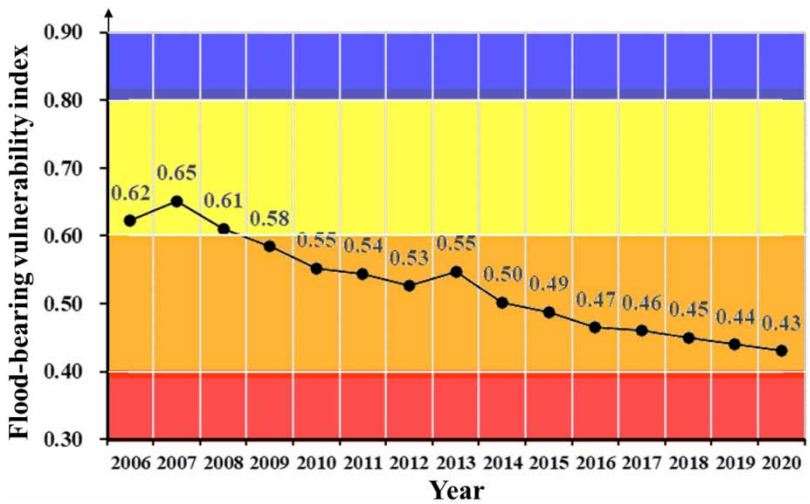

Figure 6 | Changes in the flood-bearing vulnerability index of Zhengzhou City from 2006 to 2020.

From 2006 to 2008, the flood-bearing vulnerability index at Level II increased and then decreased. Due to the strengthened drainage pipe network in 2007, the flood-bearing vulnerability was significantly reduced. From 2009 to 2020, the vulnerability index was at Level III (the second highest) and showed a significant downward trend. In 2013, the vulnerability index increased, i.e., a short-lived phenomenon of reduced flood risk. This is mainly due to the decreased urban population density in 2013 relative to 2012 and the increased disaster preparedness indicators (such as the fiscal-to-budget ratio and the drainage pipe network density).

4.3. Spatial changes in flood-bearing vulnerability of Zhengzhou City

The spatial variations of the flood-bearing vulnerability index of Zhengzhou City were analyzed by taking 2006, 2008, 2010, 2012, 2014, 2016, 2018, and 2020 as an example (Figure 7). From 2006 to 2008, the vulnerability levels of Zhongyuan, Erqi, Guancheng, and Jinshui Districts were all orange, while Huiji District was yellow. Located in the Yellow River beach area, Huiji District had a low vulnerability represented by the economy and population and a high capacity for disaster prevention and mitigation reflected by its high greening rate and river network density. With the development of urbanization, the flood-bearing vulnerability of Huiji District increased. Between 2010 and 2014, all five districts had an orange flood-bearing vulnerability level. From 2016 to 2020, the vulnerability levels of Guancheng District rose to red. In 2020, the vulnerability level of Jinshui District also rose to red.

Among the 8 years, Guancheng District had the highest flood-bearing vulnerability, while Huiji District had the lowest vulnerability. Compared with Huiji District, Guancheng District was the main urban area with a high degree of urbanization. The general disaster prevention capacity reflected in the high greening rate and drainage pipe network construction contributed to its greatest flooding vulnerability. In particular, the pipe network construction in Guancheng District was the lowest in the five districts. In 2012, the ratio of local financial income to expenditure was also severely reduced, even falling below 100%. Therefore, Guancheng District is the top priority for flood prevention and mitigation in Zhengzhou City.

5. DISCUSSION

5.1. Balanced development of urbanization and urban resilience

5.1.1. Urbanization in Zhengzhou

Rapid urbanization can cause destructive changes in the urban flood-bearing environment (Lu *et al.* 2023; Wang *et al.* 2023). From 2005 to 2020, the total scale of construction land in Zhengzhou City increased by 702 km^2; the area of watershed

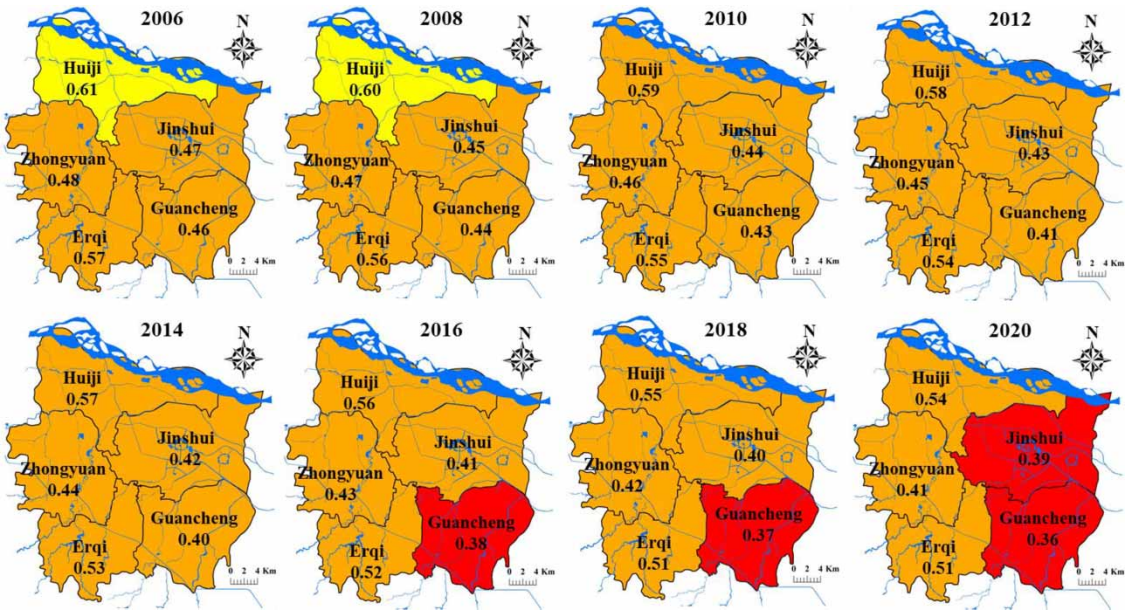

Figure 7 | Spatial variations of the flood-bearing vulnerability index for the eight typical years.

wetlands decreased by about 30% (https://tjj.zhengzhou.gov.cn/). In 2020, the resident population increased from 7.4 million in 2008 to 12.8 million. Under the constant threat of sudden extreme rainstorms, urban flood-bearing bodies and disaster-causing mechanisms significantly changed. Strengthening the management of urban flooding vulnerability is the most convenient way to cope with the double test of extreme weather and rapid urbanization.

5.1.2. Resilient urban construction in Zhengzhou

The '7.20' rainstorm and flooding significantly impacted Zhengzhou, highlighting the threats and challenges in response to climate extremes (Lv *et al.* 2022). Resilient cities play a huge role in mitigating flood damage. Urban greening can also effectively mitigate the damaging effects of flooding. Figure 8 shows that the urban greening rate in Zhengzhou City showed an annually increasing trend, which became more significant with time. However, with the surge in urban population, the greening area per capita decreased from 9.7 to 6.2 m^2. The construction of urban drainage pipe networks basically stagnated in other years, except for the dramatic increase in 2006–2007. The design standard of urban drainage pipe network was on the low side, with generally small pipe diameters. In summary, urban disaster prevention and mitigation construction lagged behind the urbanization process, resulting in insufficient urban flood control capacity. Thus, it is urgently needed to strengthen the resilient city construction in Zhengzhou City.

5.2. Urban flood prevention and mitigation policies

There are large differences in urban terrain, geographic location, elevation, and economic level. The development of urban flood resilience planning and design programs in line with their conditions can enhance the implementability and relevance of disaster prevention (Endendijk *et al.* 2023; Wang *et al.* 2023). This study proposed flood prevention planning recommendations for Zhengzhou City from three levels. (1) At the macro-city level, accurate urban flood risk maps should be prepared, and the connectivity of pipe networks and water systems should be strengthened. (2) At the meso-neighborhood level, it is important to improve the resilience of older settlements to storm flooding. (3) At the micro-household level, it is important to improve residents' own emergency response capacity and to actively implement disaster insurance.

5.3. Model performance testing

Combining different weights and evaluation models, the effectiveness and advantages of the OCM-IGTM model proposed in this article were tested through single-factor comparative experiments. The combination schemes are shown in Table 3.

Based on a single-factor comparison, only the weights or evaluation methods were changed to establish new comparative schemes. The urban flood-bearing vulnerability index is shown in Figure 9.

Their comparison results are as follows:

(1) The urban flood-bearing vulnerability index by OCM-IGTM was close to the average of each evaluation method, with a small degree of dispersion. The correlations with the other seven evaluation methods were 0.982, 0.997, 0.959, 0.984,

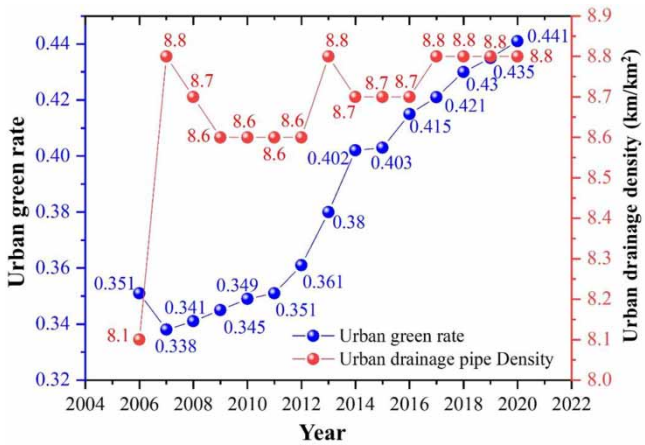

Figure 8 | Changes in greening rate and drainage pipe density in Zhengzhou City.

Table 3 | Combination schemes of different weights and evaluation models

Combination schemes			
Weighting methods	**Evaluation models**	**Combination name**	**Testing content**
OCM	Improved gray target model	OCM-IGTM	The model proposed in this article
OCM	Considering Mahalanobis distance only	OCM-mGTM	Correlation of indicators
OCM	Considering bivariate gray target only	OCM-dGTM	Significance of scheme differences
OCM	Traditional gray target model	OCM-GTM	Influence of evaluation models
AHP	Improved gray target model	AHP-IGTM	Influence of subjective weights
EW	Improved gray target model	EW-IGTM	Influence of objective weights
WLA	Improved gray target model	WLA-IGTM	Influence of combined weights

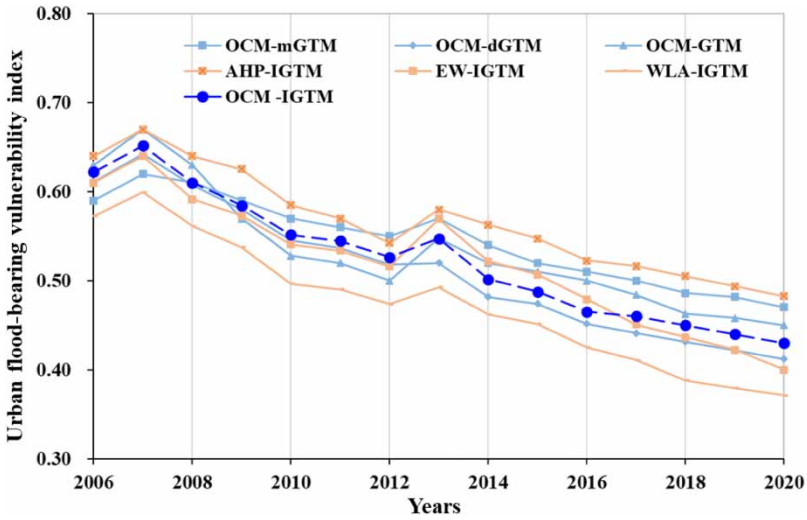

Figure 9 | Combination schemes of different weights and evaluation models.

0.974, and 0.994 (0.982 on average), respectively. It shows that the results of the OCM-IGTM model proposed in this article were reliable.

(2) The urban flood-bearing vulnerability index by the OCM-mGTM and OCM-IGTM was generally consistent with the 'maximum and minimum levels' when indicator correlations were considered. However, OCM-mGTM did not account for the significance of programmatic differences due to dual target centers. Thus, urban flood-bearing vulnerability index variability was not captured.

(3) The urban flood-bearing vulnerability index by the OCM-dGTM and OCM-IGTM was very similar, considering programmatic variability. However, OCM-dGTM did not incorporate indicator correlations, making the 'maximum and minimum levels' different from the results by most methods. Therefore, the credibility of the results obtained without considering indicator correlation was reduced.

(4) The improved gray target was adopted as an evaluation model to test the differences in results with different weights. The weights affected the absolute values of resilience more than the relative values of resilience for different years. Therefore, the evaluation results with different weights revealed the relative true values of resilience. The single subjective weighting method was greatly influenced by human factors and had certain differences in the ranking of the schemes. The single subjective weighting method was greatly influenced by human factors and had certain differences in the ranking of the schemes, with OCM-IGTM results closer to the mean of all scheme, compared with WLA-IGTM.

In conclusion, the OCM-IGTM I model constructed in this article has the following three characteristics: (1) This model takes advantage of integrating multiple independent weighting methods to determine the optimal combination of weights. (2) The Mahalanobis distance is introduced to reflect the correlation between indicators. (3) This model also incorporates the

concept of double-target criteria to represent the difference in evaluation results. These demonstrate the advantages of the OCM-IGTM model.

6. CONCLUSIONS

In order to accurately determine urban flooding vulnerability and address the defects in the index weights and GTM, this article proposed a vulnerability evaluation model for urban flooding based on the distance estimation and weighting method. The proposed model was applied to Zhengzhou City. The following main conclusions are drawn:

First, traditional gray target models have the problems of insignificant assessment of superiority and inferiority using a single bull's-eye and exclusion of indicator correlations. This article proposed the relative bull's-eye distance and introduced the Marginal distance. This can effectively address these problems and provide an important reference for improving the GTM.

Second, in order to improve the subjective and objective drawbacks of single assignment, this article proposed a method of determining optimal weights with minimizing weight deviation as the objective function based on the idea of moment estimation. This method can significantly improve the 'multiplier effect' and subjectivity in the existing combined weight scheme and provide insights into weight determination. However, the selection of the base weight set involved some subjective factors.

Finally, Zhengzhou City was taken as an example to demonstrate the proposed model. From the time scale of 2006–2020, the vulnerability to disasters in Zhengzhou City showed an upward trend. On the spatial scale (i.e., Zhengzhou's five districts), Guancheng District had the relatively highest urban flooding risk, and Huiji District had the lowest flooding risk. The imbalance between rapid urbanization and slow disaster prevention and mitigation construction in Zhengzhou was identified. Therefore, it is urgently needed to strengthen the resilient city construction in Zhengzhou.

ACKNOWLEDGEMENTS

This research was funded by the National Natural Science Foundation of China (52209038 and 52109038) and the National Key Research and Development Program of China (No. 2021YFC3200203). The authors thank the anonymous reviewers for their valuable comments.

DATA AVAILABILITY STATEMENT

All relevant data are included in the paper or its Supplementary Information.

CONFLICT OF INTEREST

The authors declare there is no conflict.

REFERENCES

Adekunle, I. A., Onanuga, A. T., Akinola, O. O. & Ogunbanjo, O. W. 2020 Modelling spatial variations of coronavirus disease (COVID-19) in Africa. *Science of The Total Environment* **729**, 138998. https://doi.org/10.1016/j.scitotenv.2020.138998.

Bucherie, A., Hultquist, C., Adamo, S., Neely, C., Ayala, F., Bazo, J. & Kruczkiewicz, A. 2022 A comparison of social vulnerability indices specific to flooding in Ecuador: Principal component analysis (PCA) and expert knowledge. *International Journal of Disaster Risk Reduction* **73**, 102897. https://doi.org/10.1016/j.ijdrr.2022.102897.

Chen, Y., Liu, T., Ge, Y., Xia, S., Yuan, Y., Li, W. & Xu, H. 2021 Examining social vulnerability to flood of affordable housing communities in Nanjing, China: Building long-term disaster resilience of low-income communities. *Sustainable Cities and Society* **71**, 102939. https://doi.org/10.1016/j.scs.2021.102939.

Chen, Q., Yu, W., Zhao, X., Nie, F. & Li, X. 2023 Rooted Mahalanobis distance based Gustafson-Kessel fuzzy C-means. *Information Sciences* **644**, 118878. https://doi.org/10.1016/j.ins.2023.03.103.

Darlington, J. C., Yiannakoulias, N. & Elshorbagy, A. 2022 Changes in social vulnerability to flooding: A quasi-experimental analysis. *Natural Hazards* **111** (3), 2487–2509. https://doi.org/10.1007/s11069-021-05145-2.

Ding, C. & Liu, T. 2023 Risk decision for a port shore power supply system based on cumulative prospect theory and an improved gray target. *Sustainability* **15** (19), 14318. https://doi.org/10.3390/su151914318.

Dong, B., Xia, J., Li, Q. & Zhou, M. 2022a Risk assessment for people and vehicles in an extreme urban flood: Case study of the '7.20' flood event in Zhengzhou, China. *International Journal of Disaster Risk Reduction* **80**, 103205. https://doi.org/10.1016/j.ijdrr.2022.103205.

Dong, X., Hu, J., Hu, C., Chen, Z. & Li, Y. 2022b Rapid identification and spectral moment estimation of non-Gaussian weather radar signal. *IEEE Transactions on Geoscience and Remote Sensing* **60**, 1–12. https://doi.org/10.1109/TGRS.2022.3168153.

Du, X., Shao, F., Wu, S., Zhang, H. & Xu, S. 2017 Water quality assessment with hierarchical cluster analysis based on Mahalanobis distance. *Environmental Monitoring and Assessment* **189**, 335. https://doi.org/10.1007/s10661-017-6035-y.

Endendijk, T., Botzen, W. J. W., de Moel, H., Aerts, J. C. J. H., Slager, K. & Kok, M. 2023 Flood vulnerability models and household flood damage mitigation measures: An econometric analysis of survey data. *Water Resources Research* **59** (8), e2022WR034192. https://doi.org/10.1029/2022WR034192.

Feloni, E., Mousadis, I. & Baltas, E. 2020 Flood vulnerability assessment using a GIS-based multi-criteria approach – The case of Attica region. *Journal of Flood Risk Management* **13** (S1), e12563. https://doi.org/10.1111/jfr3.12563.

Fu, S., Xiao, Y., Zhou, H. & Liu, S. 2021 Venture capital project selection based on interval number grey target decision model. *Soft Computing* **25**, 4865–4874. https://doi.org/10.1007/s00500-020-05495-2.

Gu, X., Zhang, Q., Li, J., Chen, D., Singh, V. P., Zhang, Y., Liu, J., Shen, Z. & Yu, H. 2020 Impacts of anthropogenic warming and uneven regional socio-economic development on global river flood risk. *Journal of Hydrology* **590**, 125262. https://doi.org/10.1016/j.jhydrol.2020.125262.

He, J. a. & Peng, F. 2022 Adaptive moment estimation for universal portfolio selection strategy. *Optimization and Engineering*. https://doi.org/10.1007/s11081-022-09776-7.

Ji, Y., Gao, D., Liu, Q., Su, J., Liu, Y., Zhao, J., Yang, Y., Fu, Y. & Huang, G. 2023 An integrated framework for agricultural non-point source pollution control technology evaluation: Application of an improved multiple attribute decision making method. *Expert Systems with Applications* **229**, 120319. https://doi.org/10.1016/j.eswa.2023.120319.

Jiang, Y., Fang, M., Liu, Z. & Wang, W. 2019 Comprehensive evaluation of power quality based on an improved TOPSIS method considering the correlation between indices. *Applied Sciences* **9** (17), 3603. https://doi.org/10.3390/app9173603.

Jibhakate, S. M., Timbadiya, P. V. & Patel, P. L. 2023 Multiparameter flood hazard, socioeconomic vulnerability and flood risk assessment for densely populated coastal city. *Journal of Environmental Management* **344**, 118405. https://doi.org/10.1016/j.jenvman.2023.118405.

Jin, H., Xu, H., Yang, S., Xu, Z., Li, F. & Hu, Z. 2020 Grey target decision analysis of optimum mixing ratio of LWAS based on the comprehensive performance. *Construction and Building Materials* **262**, 120570. https://doi.org/10.1016/j.conbuildmat.2020.120570.

Kang, S., Yin, J., Gu, L., Yang, Y., Liu, D. & Slater, L. 2023 Observation-constrained projection of flood risks and socioeconomic exposure in China. *Earth's Future* **11** (7), e2022EF003308. https://doi.org/10.1029/2022EF003308.

Kim, M., Song, K. & Chon, J. 2021 Key coastal landscape patterns for reducing flood vulnerability. *Science of The Total Environment* **759**, 143454. https://doi.org/10.1016/j.scitotenv.2020.143454.

Lai, C., Chen, X., Chen, X., Wang, Z., Wu, X. & Zhao, S. 2015 A fuzzy comprehensive evaluation model for flood risk based on the combination weight of game theory. *Natural Hazards* **77** (2), 1243–1259. https://doi.org/10.1007/s11069-015-1645-6.

Langlois, B. K., Marsh, E., Stotland, T., Simpson, R. B., Berry, K., Carroll, D. A., Ismanto, A., Koch, M. & Naumova, E. N. 2023 Usability of existing global and national data for flood related vulnerability assessment in Indonesia. *Science of The Total Environment* **873**, 162315. https://doi.org/10.1016/j.scitotenv.2023.162315.

Li, R., Jiang, Z., Ji, C., Li, A. & Yu, S. 2018 An improved risk-benefit collaborative grey target decision model and its application in the decision making of load adjustment schemes. *Energy* **156**, 387–400. https://doi.org/10.1016/j.energy.2018.05.119.

Li, J., Gao, J., Li, N., Yao, Y. & Jiang, Y. 2023a Risk assessment and management method of urban flood disaster. *Water Resources Management* **37** (5), 2001–2018. https://doi.org/10.1007/s11269-023-03467-3.

Li, Y., Ye, S., Wu, Q., Wu, Y. & Qian, S. 2023b Analysis and countermeasures of the '7.20' flood in Zhengzhou. *Journal of Asian Architecture and Building Engineering* 1–17. https://doi.org/10.1080/13467581.2023.2208195.

Liu, J., Feng, S., Gu, X., Zhang, Y., Beck, H. E., Zhang, J. & Yan, S. 2022 Global changes in floods and their drivers. *Journal of Hydrology* **614**, 128553. https://doi.org/10.1016/j.jhydrol.2022.128553.

Lu, M., Yu, Z., Hua, J., Kang, C. & Lin, Z. 2023 Spatial dependence of floods shaped by extreme rainfall under the influence of urbanization. *Science of The Total Environment* **857**, 159134. https://doi.org/10.1016/j.scitotenv.2022.159134.

Lv, H., Wu, Z., Meng, Y., Guan, X., Wang, H., Zhang, X. & Ma, B. 2022 Optimal domain scale for stochastic urban flood damage assessment considering triple spatial uncertainties. *Water Resources Research* **58** (7). https://doi.org/10.1029/2021WR031552.

Lyu, H.-M., Zhou, W.-H., Shen, S.-L. & Zhou, A.-N. 2020 Inundation risk assessment of metro system using AHP and TFN-AHP in Shenzhen. *Sustainable Cities and Society* **56**, 102103. https://doi.org/10.1016/j.scs.2020.102103.

Maskrey, S. A., Priest, S. & Mount, N. J. 2019 Towards evaluation criteria in participatory flood risk management. *Journal of Flood Risk Management* **12** (2), e12462. https://doi.org/10.1111/jfr3.12462.

Ministry of Emergency Management of the People's Republic of China (MEMPRC) 2022 *Henan Zhengzhou 7·20 Extraordinarily Heavy Rainfall Disaster Investigation Report*. Available from: https://www.mem.gov.cn/gk/sgcc/tbzdsgdcbg/202201/P020220121639049697767.pdf.

Pang, X., Gu, Y., Launiainen, S. & Guan, M. 2022 Urban hydrological responses to climate change and urbanization in cold climates. *Science of The Total Environment* **817**, 153066. https://doi.org/10.1016/j.scitotenv.2022.153066.

Peng, J. & Zhang, J. 2022 Urban flooding risk assessment based on GIS-game theory combination weight: A case study of Zhengzhou City. *International Journal of Disaster Risk Reduction* **77**, 103080. https://doi.org/10.1016/j.ijdrr.2022.103080.

Qin, B., Shi, Z., Hao, J., Liang, B., Sun, W. & He, F. 2022 Variable weight-projection gray target evaluation model of degree of protection of protective layer mining. *Energies* **15** (13). https://doi.org/10.3390/en15134654.

Ramkar, P. & Yadav, S. M. 2021 Flood risk index in data-scarce river basins using the AHP and GIS approach. *Natural Hazards* **109** (1), 1119–1140. https://doi.org/10.1007/s11069-021-04871-x.

Rentschler, J., Salhab, M. & Jafino, B. A. 2022 Flood exposure and poverty in 188 countries. *Nature Communications* **13** (1), 3527. https://doi.org/10.1038/s41467-022-30727-4.

Shukla, S. & Gedam, S. 2019 Evaluating hydrological responses to urbanization in a tropical river basin: A water resources management perspective. *Natural Resources Research* **28** (2), 327–347. https://doi.org/10.1007/s11053-018-9390-7.

Sun, R., Shi, S., Reheman, Y. & Li, S. 2022 Measurement of urban flood resilience using a quantitative model based on the correlation of vulnerability and resilience. *International Journal of Disaster Risk Reduction* **82**, 103344. https://doi.org/10.1016/j.ijdrr.2022.103344.

Tansar, H., Duan, H.-F. & Mark, O. 2023 A multi-objective decision-making framework for implementing green-grey infrastructures to enhance urban drainage system resilience. *Journal of Hydrology* **620**, 129381. https://doi.org/10.1016/j.jhydrol.2023.129381.

Tu, Y., Shi, H., Zhou, X., Liu, L. & Lev, B. 2023 Flood risk assessment of metro stations based on the SMAA-2-FFS-H method: A case study of the '7.20' rainstorm in Zhengzhou, China. *Stochastic Environmental Research and Risk Assessment* **37** (7), 2849–2868. https://doi.org/10.1007/s00477-023-02422-3.

van Schaik, M. O., Silva Mendonça, I., Cappon, H. J., Chen, W.-S. & Rijnaarts, H. H. M. 2023 Process modelling to facilitate model-based decision-making for resource recovery from urban wastewater – A grey-box approach applied to nanofiltration. *Journal of Water Process Engineering* **54**, 104014. https://doi.org/10.1016/j.jwpe.2023.104014.

Wahalathantri Buddhi, L., Lokuge, W., Karunasena, W. & Setunge, S. 2016 Vulnerability of floodways under extreme flood events. *Natural Hazards Review* **17** (1), 04015012. https://doi.org/10.1061/(ASCE)NH.1527-6996.0000194.

Wang, S., Ali, S., Yue, T. & Liaaen, M. 2018 Integrating weight assignment strategies with NSGA-II for supporting user preference multiobjective optimization. *IEEE Transactions on Evolutionary Computation* **22** (3), 378–393. https://doi.org/10.1109/TEVC.2017.2778560.

Wang, M., Fu, X., Zhang, D., Chen, F., Liu, M., Zhou, S., Su, J. & Tan, S. K. 2023 Assessing urban flooding risk in response to climate change and urbanization based on shared socio-economic pathways. *Science of The Total Environment* **880**, 163470. https://doi.org/10.1016/j.scitotenv.2023.163470.

Wen, Q., Liu, G., Wu, W. & Liao, S. 2021 Multicriteria comprehensive evaluation framework for industrial park-level distributed energy system considering weights uncertainties. *Journal of Cleaner Production* **282**, 124530. https://doi.org/10.1016/j.jclepro.2020.124530.

Wing, O. E. J., Pinter, N., Bates, P. D. & Kousky, C. 2020 New insights into US flood vulnerability revealed from flood insurance big data. *Nature Communications* **11** (1), 1444. https://doi.org/10.1038/s41467-020-15264-2.

Xing, Z., Yang, S., Zan, X., Dong, X., Yao, Y., Liu, Z. & Zhang, X. 2023 Flood vulnerability assessment of urban buildings based on integrating high-resolution remote sensing and street view images. *Sustainable Cities and Society* **92**, 104467. https://doi.org/10.1016/j.scs.2023.104467.

Xu, H., Ma, C., Lian, J., Xu, K. & Chaima, E. 2018 Urban flooding risk assessment based on an integrated k-means cluster algorithm and improved entropy weight method in the region of Haikou, China. *Journal of Hydrology* **563**, 975–986. https://doi.org/10.1016/j.jhydrol.2018.06.060.

Yang, W., Zhang, J. & Krebs, P. 2023 Investigating flood exposure induced socioeconomic risk and mitigation strategy under climate change and urbanization at a city scale. *Journal of Cleaner Production* **387**, 135929. https://doi.org/10.1016/j.jclepro.2023.135929.

Ye, F., Sun, J., Wang, Y., Nedjah, N. & Bu, W. 2023 A novel method for the performance evaluation of institutionalized collaborative innovation using an improved G1-CRITIC comprehensive evaluation model. *Journal of Innovation & Knowledge* **8** (1), 100289. https://doi.org/10.1016/j.jik.2022.100289.

Zhang, W., Villarini, G., Vecchi, G. A. & Smith, J. A. 2018 Urbanization exacerbated the rainfall and flooding caused by hurricane Harvey in Houston. *Nature* **563** (7731), 384–388. https://doi.org/10.1038/s41586-018-0676-z.

Zhang, H., Zhang, J., Fang, H. & Yang, F. 2022 Urban flooding response to rainstorm scenarios under different return period types. *Sustainable Cities and Society* **87**, 104184. https://doi.org/10.1016/j.scs.2022.104184.

Zheng, Q., Shen, S.-L., Zhou, A. & Lyu, H.-M. 2022 Inundation risk assessment based on G-DEMATEL-AHP and its application to Zhengzhou flooding disaster. *Sustainable Cities and Society* **86**, 104138. https://doi.org/10.1016/j.scs.2022.104138.

Zhu, X. & Wen, H. 2023 Application of multi-index grey target decision method in prediction of coal temperature in goaf. *Combustion Science and Technology* 1–15. https://doi.org/10.1080/00102202.2023.2177510.

Zia, A., Rana, I. A., Arshad, H. S. H., Khalid, Z. & Nawaz, A. 2023 Monsoon flood risks in urban areas of Pakistan: A way forward for risk reduction and adaptation planning. *Journal of Environmental Management* **336**, 117652. https://doi.org/10.1016/j.jenvman.2023.117652.

Ziarh, G. F., Asaduzzaman, M., Dewan, A., Nashwan, M. S. & Shahid, S. 2021 Integration of catastrophe and entropy theories for flood risk mapping in peninsular Malaysia. *Journal of Flood Risk Management* **14** (1), e12686. https://doi.org/10.1111/jfr3.12686.

First received 18 March 2024; accepted in revised form 11 July 2024. Available online 22 July 2024